BIOCHEMISTRY

A chimeric membrane enzyme and an engineered whole-cell biocatalyst for efficient 1-alkene production

Tabish Iqbal, Subhashini Murugan, Debasis Das*

Bioproduction of 1-alkenes from naturally abundant free fatty acids offers a promising avenue toward the next generation of hydrocarbon-based biofuels and green commodity chemicals. UndB is the only known membrane-bound 1-alkene–producing enzyme, with great potential for 1-alkene bioproduction, but the enzyme exhibits limited turnovers, thus restricting its widespread usage. Here, we explore the molecular basis of the limitation of UndB activity and substantially improve its catalytic power. We establish that the enzyme undergoes peroxide-mediated rapid inactivation during catalysis. To counteract this inactivation, we engineered a chimeric membrane enzyme by conjugating UndB with catalase that protected UndB against peroxide and enhanced its number of turnovers tremendously. Notably, our chimeric enzyme is the only example of a membrane enzyme successfully engineered with catalase. We subsequently constructed a whole-cell biocatalytic system and achieved remarkable efficiencies (up to 95%) in the biotransformation of a wide range of fatty acids (both aliphatic and aromatic) into corresponding 1-alkenes with numerous biotechnological applications.

INTRODUCTION

The steep increase in the demand for fuels, coupled with the finite availability of fossil fuels, is driving the exploration of sustainable fuel pathways, spurring immense interest in developing renewable and eco-friendly biofuels. Since hydrocarbons are the major constituents of fossil fuels, their sustainable biosynthesis presents a promising avenue toward the next generation of hydrocarbon-based biofuels (*1*–*4*). Notably, the medium-chain 1-alkenes are promising biofuel candidates because of their exceptional properties, including low freezing point, high energy content, recovery convenience due to their insolubility in water, and compatibility with current engine systems and transportation infrastructures (*5*). 1-Alkenes are also heavily used as commodity chemicals in various industries as precursors of detergents, polymers, and lubricants (*6*–*10*), making them attractive molecules to biosynthesize. A feasible route to 1-alkene biosynthesis is the enzymatic one-step decarboxylation of naturally abundant free fatty acids by fatty acid decarboxylases (*11*, *12*). These enzymes include a heme-containing soluble cytochrome P450 enzyme, OleT (*13*); a soluble non-heme diiron enzyme, UndA (*14*, *15*); and a recently explored integral membrane enzyme, UndB (*16*, *17*). While OleT prefers long-chain fatty acids (*13*), with the medium-chain fatty acids (C6 to C12), the enzyme exhibits compromised chemoselectivity, producing undesirable hydroxy fatty acids as side products (*18*). In contrast, UndA and UndB prefer medium-chain fatty acids, producing medium-chain 1-alkenes that are biotechnologically attractive molecules (*14*, *16*, *17*). Notably, the sluggish nature of UndA and its narrow substrate scope pose great challenges to its use for the efficient production of medium-chain 1-alkenes (*14*).

The discovery of UndB, the only known membrane-bound fatty acid decarboxylase, has added enhanced interest in using this enzyme for the biosynthesis of medium-chain 1-alkenes (*16*). Previous studies have demonstrated that UndB has a broader substrate range (C6 to C18) and notably better activity than UndA (*16*, *19*). However, the properties of UndB remained poorly understood for nearly a decade, primarily due to the membrane-bound nature of the enzyme.

Department of Inorganic and Physical Chemistry, Indian Institute of Science, Bangalore, Karnataka 560012, India.
*Corresponding author. Email: debasisdas@iisc.ac.in

Recently, we reported the detailed biochemical characterization of UndB (*17*). Using the purified full-length enzyme, we demonstrated that UndB is an integral membrane non-heme diiron enzyme that catalyzes the oxidative decarboxylation of free fatty acids to terminal alkenes (Fig. 1). We established that UndB converts a broad range of fatty acids (C10 to C18) to the corresponding 1-alkenes. The greatest activity of the enzyme was observed with lauric acid (C12 fatty acid). UndB activity was dependent on redox partners such as NADPH (reduced form of $NADP^+$)/ferredoxin (Fdx)/ferredoxin reductase (FNR) (Fig. 1) (*17*). UndB was more effective than UndA and OleT in producing 1-undecene. However, we observed that the activity of the purified UndB stalled within 1 min, with the total turnover numbers (TTN) being only 14, limiting its scope for applications and underscoring the necessity to uncover the origin of enzyme inactivation and finding means to counter it. However, such investigation is challenging due to the recalcitrant membrane-bound nature of the enzyme.

Here, we demonstrate that the mechanism of UndB inactivation involves the inhibition by hydrogen peroxide (H_2O_2) produced in situ by an uncoupled electron transfer step to molecular oxygen during the enzyme reaction (Fig. 1, unproductive pathway, red arrows). We found that the H_2O_2 inhibition of UndB is reversible and can be countered by catalase. We engineered a chimeric membrane enzyme by conjugating UndB with catalase, with the chimera exhibiting a remarkably improved number of catalytic turnovers of fatty acids to 1-alkenes. Further, we constructed a state-of-the-art whole-cell biocatalyst that enabled highly efficient biotransformation of a wide range of aliphatic and aromatic fatty acids to terminal alkenes. Our findings demonstrate the potential of UndB as an efficient tool for the preparative scale production of valuable medium-chain 1-alkenes with diverse industrial applications.

RESULTS

Origin of limited turnovers of UndB

The serendipitous discovery (*16*) and the recent investigation of UndB (*17*), a member of fatty acid desaturase (FADS)–like superfamily, have revealed several unique catalytic properties of the enzyme. Among the members of the FADS-like superfamily, UndB is

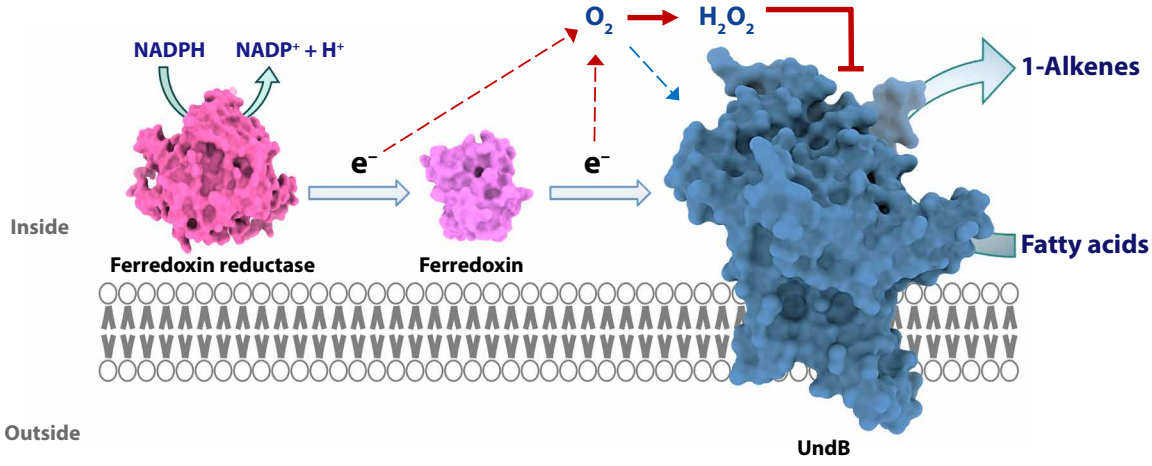

Fig. 1. Schematic illustrations of the redox-dependent conversion of fatty acids to 1-alkenes by UndB. The UndB reaction requires electrons, mediated by redox partners such as Fdx/FNR/NADPH system (productive pathway, blue arrows). In this study, we discovered that UndB is inactivated by H_2O_2, produced in situ by uncoupled electron transfer from the redox partners to O_2 (unproductive pathway, red arrows). The details of the protein structures are described in Materials and Methods. For UndB, the transmembrane domain was predicted using the Deep-TMHMM tool (*38*).

the only known enzyme capable of converting free fatty acids to 1-alkenes, making it an attractive candidate for potential biotechnological applications. Our recent study has illustrated that UndB requires molecular oxygen (O_2) and redox partners (NADPH/FNR/Fdx) for catalysis (*17*). The catalytic rate of UndB was substantially greater than OleT and UndA in converting medium-chain fatty acids to 1-alkenes. However, despite the initial optimism about UndB, the purified enzyme in detergent exhibited poor activity (14 TTN) and stalled in 1 min (*17*).

To probe this poor activity of UndB, we explored the biotransformation of lauric acid to 1-undecene by UndB at various stages of the enzyme preparation, including the whole cells, cell lysates, membrane fractions, and spheroplast preparations (Fig. 2A), a recently promoted preparation for biotransformation by membrane-bound enzymes (*20*). UndB exhibited prolonged activity in all these preparations compared to the purified enzyme. While the purified enzyme was stalled within 1 min, the enzyme activity within the whole cells persisted for 40 min (Fig. 2B), leading to substantially greater values of TTN (Fig. 2C). Therefore, we hypothesized that the lower activity of purified UndB could be due to the separation of the enzyme from the native membrane lipids, inducing protein instability—a phenomenon often observed with detergent-purified membrane proteins (*21*–*23*).

To test whether UndB loses its stability upon purification in detergents, we compared the thermal stability of the detergent-purified UndB and the enzyme in the whole-cell lysates by measuring the relative activity of the enzyme upon providing thermal stress in a range of temperatures. Unexpectedly, purified UndB exhibited a melting temperature (T_m) 46° ± 1°C, a value close to the T_m of UndB in the whole-cell lysate (49° ± 1°C) (Fig. 3, A and B), suggesting that loss of the lipid environment due to detergent purification is not the reason of UndB inactivation. Therefore, the limited activity of purified UndB could be attributed to either exhaustion of assay components or enzyme inhibition during catalysis. We supplemented the enzyme reaction with each assay component, individually or collectively, as the number of turnovers approached the maximum. We found that the addition of Fdx, FNR, and NADPH—either alone or in combination—did not enhance the TTN of UndB (Fig. 3C). Notably, the addition of an equimolar amount of UndB into the reaction resulted in the linear proceeding of reaction for about 2 min and yielding nearly twice the product in initial 2 min (Fig. 3C). This observation suggests that inhibition of UndB occurs during catalysis. We hypothesized that the involvement of noncognate redox partners (cyanobacterial Fdx/FNR) in the aerobic UndB reaction could lead to uncoupled electron transfer from NADPH to O_2 via FNR/Fdx, resulting in the in situ generation of reactive oxygen species (ROS) that could inactivate UndB.

Previously, we demonstrated that UndB could not use H_2O_2 as a replacement for O_2 and external electrons when performing the catalysis, suggesting that the peroxide shunt pathway does not operate for UndB catalysis (*17*). To extend this observation, we included H_2O_2 in the UndB reaction in the presence of the redox partners that support multiple turnovers of the enzyme. Unexpectedly, no product was observed in the presence of H_2O_2, demonstrating that UndB was inhibited by H_2O_2 (Fig. 3D). This observation suggested the production of H_2O_2 as ROS during UndB catalysis. To substantiate the in situ production of H_2O_2, we attempted to detect it in the UndB reaction. Using the amplex red hydrogen peroxide/peroxidase assay, we found that 139 ± 3 μM H_2O_2 was formed in the standard UndB reaction (Fig. 3E). In contrast, no H_2O_2 was detected upon omission of NADPH from the assay (Fig. 3E). The amount of H_2O_2 production in the UndB reaction was very substantial, corresponding to the uncoupled electron transfer of the majority of the NADPH electrons to O_2 in the reaction (fig. S1).

We also explored whether superoxide could also contribute to UndB inhibition. We investigated the activity of UndB in the presence of superoxide dismutase (SOD) that efficiently metabolizes superoxide. We found that the addition of SOD to UndB reaction did not affect the enzyme activity, confirming that superoxide is not involved in UndB inhibition (fig. S2). These findings suggested H_2O_2-mediated rapid inhibition of UndB during catalysis. Therefore, we focused on rescuing the enzyme activity by protecting it from H_2O_2 inhibition.

Enhancing UndB activity by rescuing it from H_2O_2 inhibition

To further validate the H_2O_2-mediated inhibition of UndB, we introduced catalase to a UndB reaction that was stalled by the pretreatment

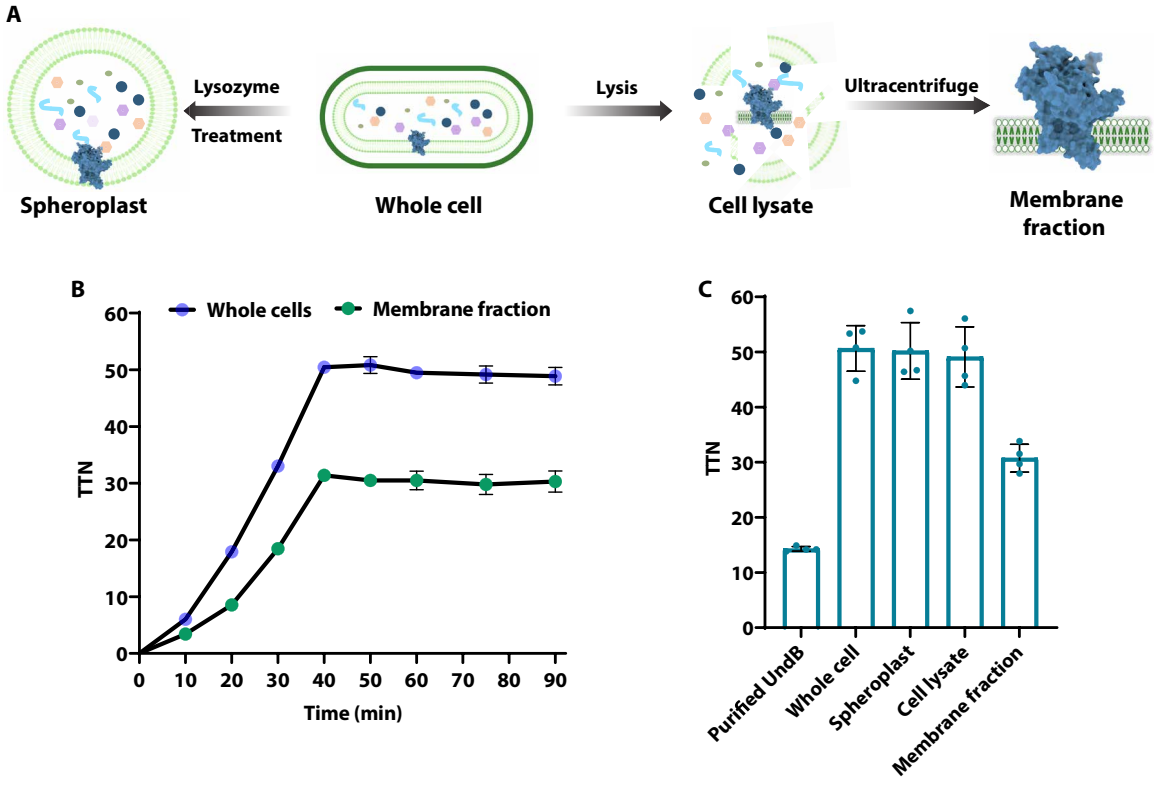

Fig. 2. UndB-catalyzed biotransformation of lauric acid to 1-undecene. (**A**) Schematic representation of UndB preparations used for the biotransformation of lauric acid to 1-undecene. (**B**) Time course of UndB reaction using whole cells and membrane fractions. (**C**) Comparative end-point activity analysis of purified UndB with whole cells, spheroplast preparations, cell lysates, and isolated membrane fractions harboring UndB. Assays were performed with UndB expressed with enhanced green fluorescent protein (eGFP) fusion (see Materials and Methods), and protein concentrations were measured by the fluorescence intensities (*39*). Assays were performed with 5 μM enzyme in each preparation in the presence of 500 μM lauric acid and 2 mM ascorbate. Experiments were performed at 25°C for the indicated time points or up to 1 hour for the end-point TTN determination. Error bars in (B) represent the standard deviation (SD) of two experiments performed in triplicate ($n = 6$). Error bars in (C) represent the SD of quartet ($n = 4$) data.

with exogenous H_2O_2. Catalase efficiently disproportionates H_2O_2 into O_2 and H_2O. Notably, the inclusion of catalase led to the recovery of UndB activity and also led to a substantial boost to the TTN of UndB to 65 ± 3, which is a 4.7-fold increase in the UndB activity compared to the standard reaction (Fig. 3D). This finding suggests that the H_2O_2 inhibition of UndB is reversible. To further elaborate, we added catalase at different time points to the standard UndB reaction in the absence of exogenous H_2O_2. We observed that the addition of catalase rescued the enzyme from inhibition at each time point, confirming the reversible nature of H_2O_2 inhibition (Fig. 3F). In the presence of catalase, H_2O_2 concentration in the UndB reaction was negligible, suggesting rapid disproportionation of H_2O_2 by catalase (Fig. 3E). Further, the inclusion of sodium azide, a potent inhibitor of catalase (*24*, *25*), restored the H_2O_2 in the UndB assays (Fig. 3E), leading to enzyme inactivation and confirming in situ generation of H_2O_2 in the UndB reaction.

Next, we investigated UndB activity in the presence of catalase without adding exogenous H_2O_2 to the reaction. We observed that the addition of catalase led to a substantial increase in the TTN of UndB to 185 ± 3. Subsequently, we systematically optimized the catalase-assisted UndB reaction conditions (fig. S3) and achieved a TTN of 265 ± 2 (Fig. 3D), which is a 19-fold enhancement in UndB activity compared to the starting 14 TTN of UndB. To our knowledge, this is the greatest TTN achieved for lauric acid decarboxylation with the 1-undecene–producing enzymes. To validate this result, we performed a comparative study of 1-undecene production by UndB, UndA, and OleT, under their optimal reaction conditions (*14*, *26*). Furthermore, we used OleT fused with an endogenously H_2O_2-producing system alditol oxidase (AldO), as described previously, for the comparative analysis (*27*). For this purpose, we heterologously expressed UndA, OleT, and OleT-AldO in *Escherichia coli* and purified them to homogeneity (figs. S4 and S5). While UndA exhibited poor activity, UndB, OleT, and OleT-AldO showed substantial 1-undecene production (fig. S6). The poor activity of UndA is possibly due to the cofactor instability, as proposed earlier (*28*). The TTN achieved with UndB was 3.9-fold greater than OleT used with the CamAB system (redox partner proteins for OleT, described in the Supplementary Materials) and 1.9-fold greater than the OleT-AldO system (fig. S6). It should be noted that OleT is also known to produce unwanted side products such as hydroxy fatty acids (*12*). Our study demonstrates that UndB is the most effective 1-undecene–producing enzyme and highlights the critical role of catalase in bolstering the high activity of UndB.

Kinetic characterization of catalase-assisted UndB catalysis

We followed the time course of UndB in the presence of catalase and found that the reaction persisted for 40 min (Fig. 4A), notably

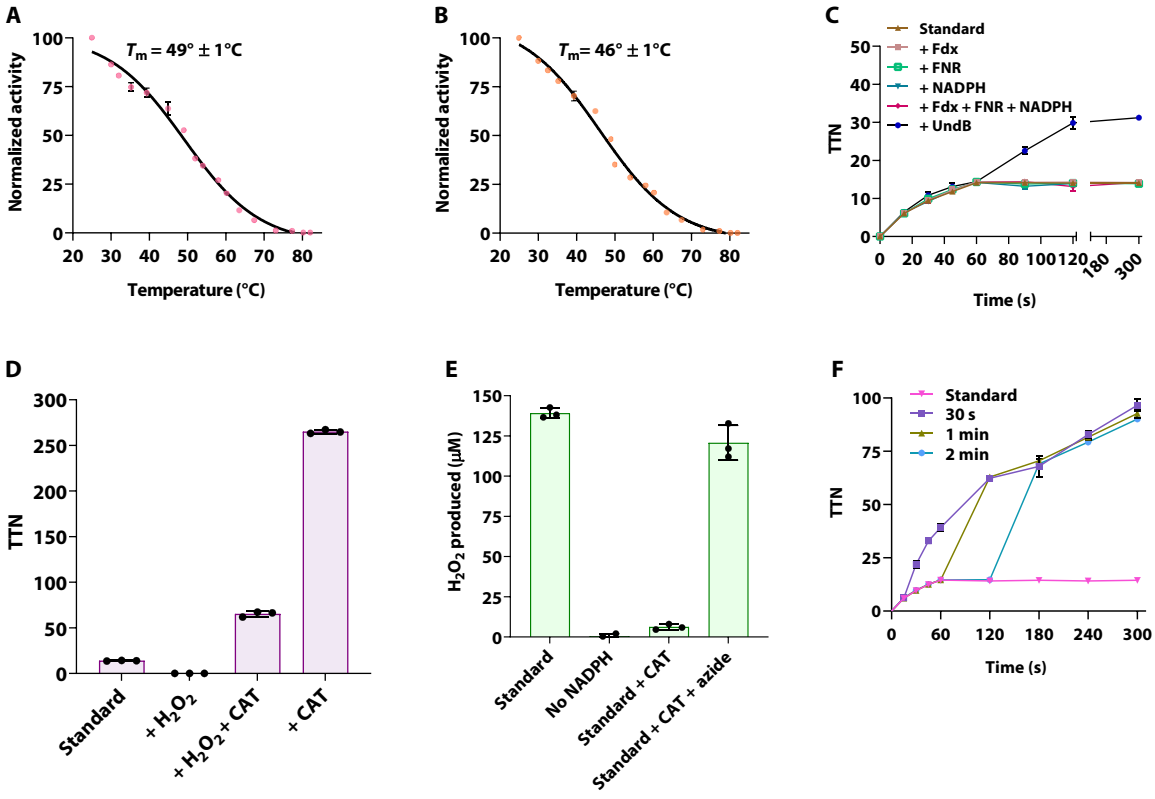

Fig. 3. Inhibition of UndB during catalysis and protection against the inhibition. Thermal denaturation curve of UndB in (**A**) whole-cell lysates and (**B**) detergent-purified form. The activities of UndB presented in panels (A) and (B) resulted from assays performed with UndB expressed with eGFP fusion, and protein concentrations were measured by the fluorescence intensities. The protein concentration used was 5 μM. After heating the sample at the indicated temperature (see Materials and Methods), the sample was cooled, and the assay was performed at 25°C. (**C**) TTN of UndB upon adding various assay components to the UndB reaction at the time point when the reaction stalls (1 min). (**D**) Effect of H_2O_2 and catalase (CAT) on UndB activity. (**E**) Detection of H_2O_2 in the UndB reaction. (**F**) Effect of addition of catalase on the UndB activity at different time points. Assays were performed at 25°C. Error bars in (A) to (F) represent the SD of triplicate ($n = 3$) data.

similar to the UndB time course in the whole cells or membrane fractions and in contrast to the standard UndB reaction with purified enzyme that stalled in 1 min without catalase. The finding of the catalase-assisted enhancement of UndB activity allowed us to conduct screening of the redox partners and a rigorous kinetic analysis of UndB. We assessed the catalase-assisted activity of UndB in the presence of *Synechococcus elongatus* (strain PCC 7942) Fdx/FNR pair, Fdx from *Prochlorococcus marinus* MIT9313 (*Pma*-Fdx) paired with FNR, putidaredoxin/putidaredoxin reductase (Pdx/PdR) pair from *Pseudomonas putida*, and cytochrome b_5/cytochrome b_5 reductase (Cytb5/Cytb5R) from *Arabidopsis thaliana* (see the Supplementary Materials for details). In the presence of catalase, we observed an overall increase in UndB activity with all the redox couples (Fig. 4B). Further, we observed greater activity of UndB when using Fdx/FNR than the other redox couples. Under these optimized conditions, we probed the substrate specificity of UndB in the presence of catalase by measuring the kinetics of the enzyme with fatty acids of various chain lengths. We found that UndB has the greatest catalytic efficiency (k_{cat}/K_m) with lauric acid (Fig. 4C). Notably, the addition of catalase to the assay enhanced the UndB activity with other fatty acids as well. The turnover numbers (k_{cat}) of UndB for the shorter-chain fatty acids (C10 to C11) were lower than that for lauric acid but greater than that for longer-chain fatty acids (C16 to C18) (Fig. 4C). It is noteworthy that although the addition of catalase rescued UndB from H_2O_2 inhibition, it did not limit the uncoupling of electrons. We observed nearly four equivalents of NADPH consumption per mole of product formed (fig. S7). Nevertheless, our study provides the basis for further engineering the system and finding the native redox partners of UndB for effective electron transfer.

Engineering the chimeric membrane enzyme, KatE-UndB

Catalase-assisted reversal of UndB inhibition and substantial enhancement of enzyme activity provided us with the opportunity to use UndB for efficient biotransformation of free fatty acids to 1-alkenes. However, efficient 1-alkenes production using a whole-cell biocatalyst requires that UndB be proximal to catalase to ensure sustained enzyme activity in the complex cellular milieu. Therefore, we designed and engineered a chimeric protein, KatE-UndB, where KatE (catalase HPII from *E. coli*) is conjugated to the N terminus of UndB (Fig. 5A) (see Materials and Methods and the Supplementary Materials for the details of the genetic construct). We expressed the chimeric protein in *E. coli*. The KatE-UndB chimeric protein retained the localization of UndB to the cell membrane, and the purification was performed with the aid of detergent (see Materials and Methods). The purified protein exhibited a single band on the SDS–polyacrylamide

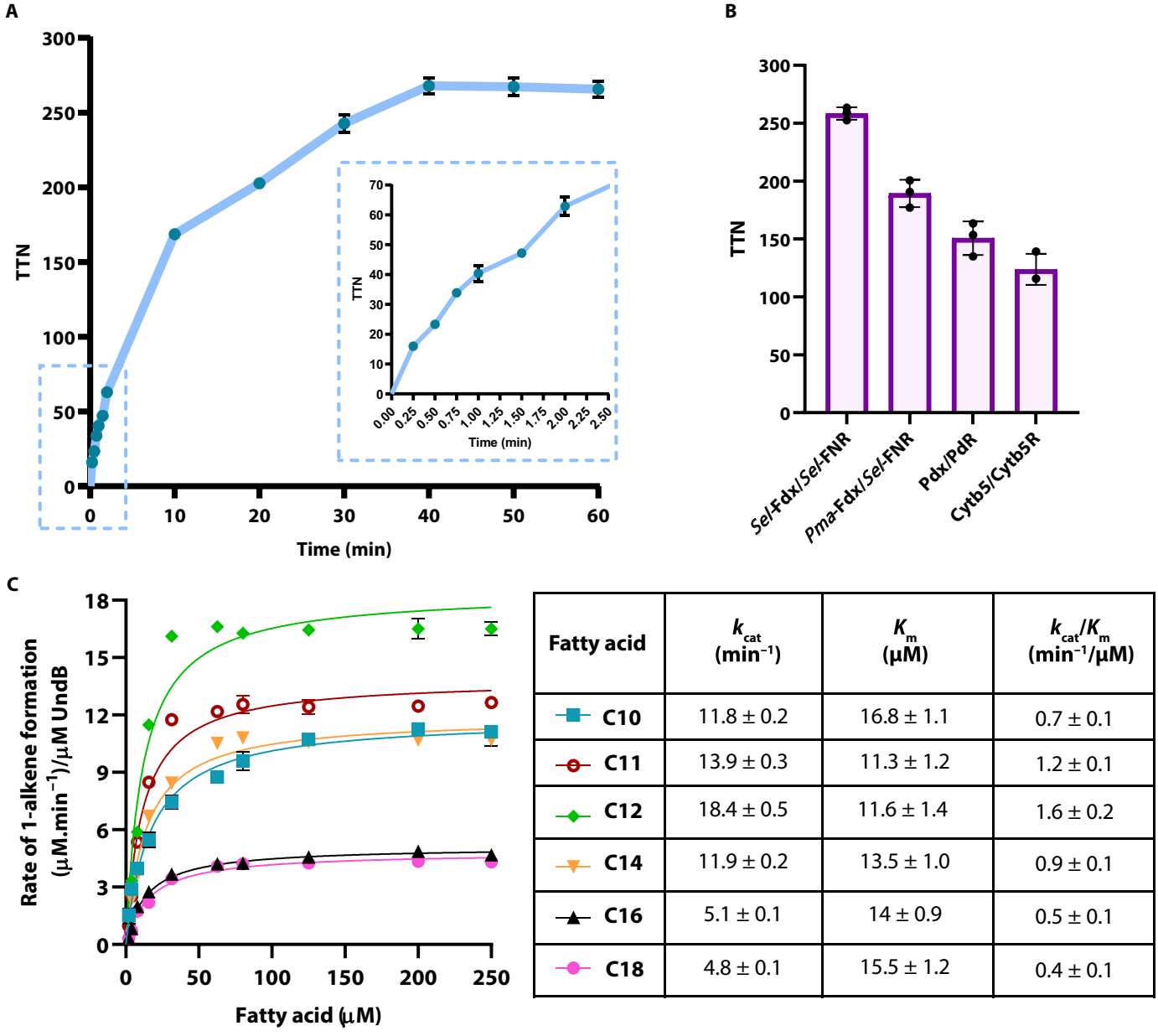

Fatty acid	k_{cat} (min^{-1})	K_m (μM)	k_{cat}/K_m (min^{-1}/μM)
C10	11.8 ± 0.2	16.8 ± 1.1	0.7 ± 0.1
C11	13.9 ± 0.3	11.3 ± 1.2	1.2 ± 0.1
C12	18.4 ± 0.5	11.6 ± 1.4	1.6 ± 0.2
C14	11.9 ± 0.2	13.5 ± 1.0	0.9 ± 0.1
C16	5.1 ± 0.1	14 ± 0.9	0.5 ± 0.1
C18	4.8 ± 0.1	15.5 ± 1.2	0.4 ± 0.1

Fig. 4. Catalase-assisted UndB catalysis. (**A**) Time course of the UndB reaction in the presence of catalase (inset: expansion of the short time course region of the UndB reaction). (**B**) Redox partner screening for the UndB activity in the presence of catalase. (**C**) Michaelis-Menten kinetics of UndB with fatty acids of various chain lengths (left). The kinetic parameters are mentioned in the associated table (right). The individual curves are presented in figs. S23 to S28. All assays were performed at 25°C with 0.5 μM purified UndB in the presence of catalase (1 mg/ml). The kinetic parameters presented in (C) were determined by measuring the initial rates after 10 min of the reaction. Error bars in (A) to (C) represent the SD of triplicate data ($n = 3$).

gel electrophoresis (SDS-PAGE) (Fig. 5B) and eluted as a single peak during the size exclusion chromatography (SEC) (fig. S8A), demonstrating the homogeneity of the purified chimeric protein. The ultraviolet (UV)–visible spectrum of the purified protein exhibited a peak at 405 nm, corresponding to the Soret band of heme (*29*), confirming the presence of heme-containing catalase in the chimeric protein (fig. S8B).

We subsequently explored the activity of KatE-UndB using lauric acid to confirm that both partners of the chimeric protein are active. We observed that the chimeric protein exhibits TTN of 271 ± 2 (Fig. 5C), which is nearly identical to the TTN observed with the purified UndB in the presence of exogenous catalase. Further, the time course analysis of the KatE-UndB activity revealed that the enzyme sustains activity for 40 min (Fig. 5C), similar to the time course of purified UndB with exogenous catalase. Notably, the inclusion of exogenous catalase in the KatE-UndB assay did not improve the TTN (fig. S9), demonstrating that the UndB conjugated catalase is active and effectively supports the UndB activity. The successful

construction of a fully functional chimeric membrane enzyme composed of KatE (for detoxification of in situ–produced H_2O_2) and UndB (for fatty acid decarboxylation) allowed us to use the construct for developing a unique whole-cell biocatalyst for efficient biotransformation of free fatty acids to terminal alkenes.

Engineering a whole-cell biocatalyst for efficient 1-alkene production

The *E. coli* cells expressing UndB (referred to as *strain-U*) (fig. S10A) catalyzed the biotransformation of lauric acid to 1-undecene for up to 40 min (Fig. 2B). The time course of catalase-supported in vitro activities of the purified UndB and the chimeric KatE-UndB was also 40 min (Figs. 4A and 5C), suggesting that the bacterial endogenous catalase may support UndB activity in whole cells. However, *strain-U* exhibited a TTN of 51 ± 4 (Fig. 2C), which is substantially lower than the TTN (271 ± 2) of the chimeric KatE-UndB (Fig. 5C). Such a difference could be attributed to differences in the expression of UndB and the endogenous catalase of *E. coli*, which might not provide sufficient protection to UndB from H_2O_2. We rationalized that the chimeric KatE-UndB could minimize the detrimental effects of H_2O_2 and exhibit better activity in whole cells than the UndB alone. Therefore, we expressed the chimeric KatE-UndB in *E. coli* to generate the *strain-KU* (fig. S10B) and compared its activity to produce 1-undecene from lauric acid with *strain-U* (fig. S10A). We found that *strain-KU* exhibits a conversion of 28%, which is nearly twofold greater than the conversion with *strain-U* (14%) (Fig. 6A).

To further improve the strains for more efficient 1-undecene production, we introduced the genes encoding Fdx/FNR from *S. elongatus*, which supported the greatest in vitro activity of UndB, to *strain-KU* to generate the *strain-KUF* (fig. S10C). To *strain-KU*, we also incorporated genes encoding Pdx and PdR from *P. putida*, which were reported to improve the in vivo production of 1-alkenes (*19*), to generate the *strain-KUP* (fig. S10D).

Both the engineered strains exhibited substantially improved 1-undecene production when compared to the *strain-KU*. While the *strain-KUP* showed 61 ± 2% conversion of lauric acid to 1-undecene, *strain-KUF* showed a remarkable 95 ± 1% conversion (Fig. 6A). A comparative time course study of the *strain-U*, *strain-KU*, and *strain-KUF* demonstrated that the *strain-KUF* has the greatest rate of 1-undecene production from lauric acid (Fig. 6B), suggesting the synergistic effect of adequate electron transfer via FNR/Fdx and the protection of UndB against H_2O_2 by the conjugated catalase by means of protection via inhibitor metabolism (PIM) mechanism (*30*). Overall, we successfully developed an engineered *E. coli* strain capable of producing 1-undecene from lauric acid with very high efficiency.

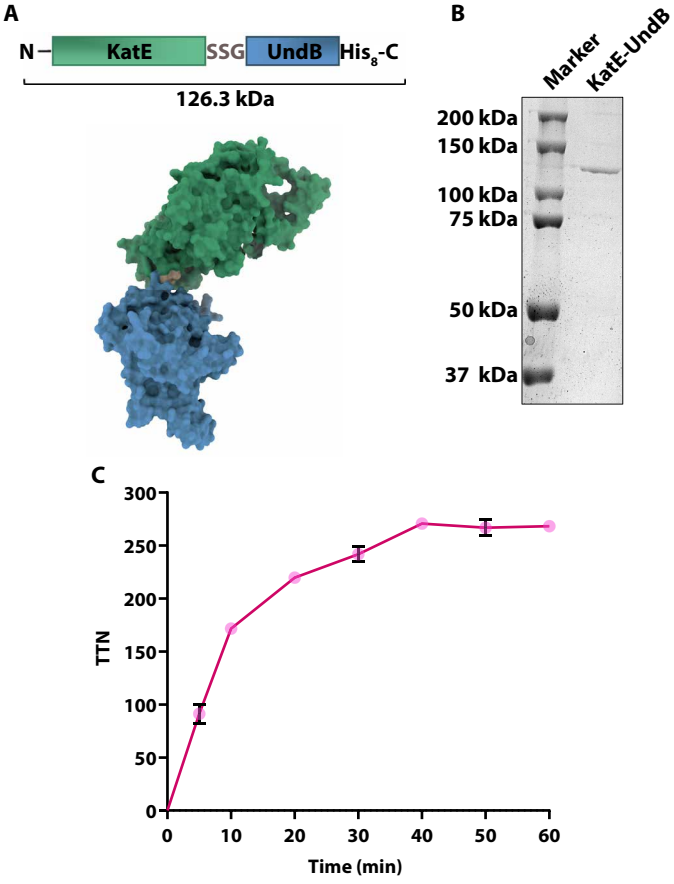

Fig. 5. Purification and activity analysis of chimeric KatE-UndB. (**A**) Schematic of the chimeric protein KatE-UndB used in this study. The structure of the chimeric protein was modeled using AlphaFold2 as described in Materials and Methods. (**B**) SDS-PAGE analysis of the purified KatE-UndB. (**C**) Time course activity of chimeric KatE-UndB. Assays were performed at 25°C with 0.5 μM purified chimeric protein. Error bars in (C) represent the SD of triplicate ($n = 3$) data.

Efficient microbial production of aliphatic and aromatic 1-alkenes

The engineered *strain-KUF* showed a remarkable 95 ± 1% conversion in a preparative scale conversion of lauric acid (**5**) feed (1 mM) to 1-undecene (Figs. 6A and 7). We subsequently explored the scope for application of the developed *strain-KUF* in the biotransformation of a range of aliphatic and aromatic fatty acids. Further, we compared the biotransformation of fatty acids to 1-alkenes by the *strain-KUF* with the *E. coli* cells expressing OleT with Pdx/PdR (referred to as *strain-OP*) and UndA (referred to as *strain-UndA*) (see Materials and Methods), the other known 1-alkene producing fatty acid decarboxylases (Fig. 7). We also tested *strain-OA*, the *E. coli* strain expressing OleT-AldO chimeric protein; however, *strain-OA* exhibited poor activity compared to *strain-OP* (fig. S11). Therefore, we used *strain-OP* for further studies (Fig. 7 and figs. S11 to S21). Notably, *strain-KUF* exhibited substantially better production of a range of aliphatic 1-alkenes (**1a** to **6a**) from the corresponding fatty acids than the other two strains (Fig. 7 and figs. S11 to S18). It is important to note that the production of the short-chain aliphatic 1-alkenes (C5 to C7) (**1a** to **2a**) by *E. coli* cells expressing UndB, which were meager in the previous report (*16*), were substantially improved (20 to 43% conversion) when using the *strain-KUF* (Fig. 7). We observed an improvement of 8.8-fold in 1-pentene production and 13-fold in 1-heptene production by *strain-KUF* over *strain-U* (figs. S12 and S13). *Strain-KUF* was also able to convert the longer-chain aliphatic fatty acids (C16 to C18) (**7** to **8**) to corresponding 1-alkenes (**7a** to **8a**) (Fig. 7 and figs. S17 and S18) better than *strain-OP* harboring OleT that is known to be more specific toward these substrates (*13*).

Notably, we did not observe any apparent adverse effect of the added substrate and the ensuing product on the growth of *strain-KUF* (fig. S22). Further, we observed that despite exhibiting lower expression levels of KatE-UndB (in *strain-KUF*) compared to UndA (in *strain-UndA*) and OleT (in *strain-OP*), the *strain-KUF* showed better

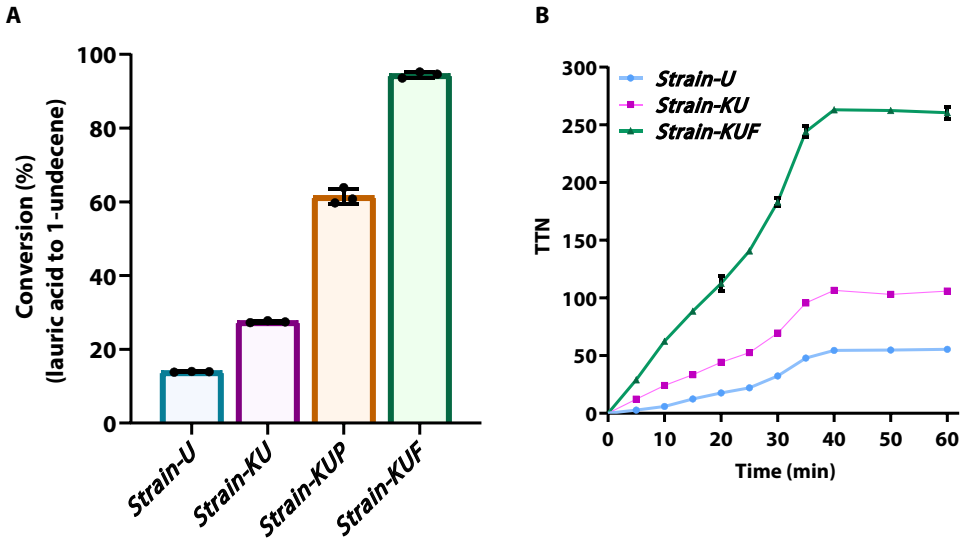

Fig. 6. Activity analysis of the microbial strains developed for biotransformation studies. (**A**) Percentage conversion of lauric acid to 1-undecene using various strains. Experiments were performed on a preparative scale where 1 mM lauric acid was fed to the cultures. Error bars in (A) represent the SD of triplicate data ($n = 3$). (**B**) Time course of 1-undecene production using the *strain-U*, *strain-KU*, and *strain-KUF*. Error bars in (B) represent the SD of two experiments performed in triplicate ($n = 6$).

conversion rates of fatty acids to 1-alkenes compared to *strain-UndA* and *strain-OP*. Such efficacy of *strain-KUF* could be attributed to the synergistic effect of the engineered *strain-KUF* coupled with the membrane localization of UndB. The positioning of UndB in the cell membrane may lead to the facile access of UndB to fatty acids, potentially contributing to its superior conversion efficiency compared to the other two enzymes expressed in the cytoplasm of bacterial cells.

The broad substrate specificity of *strain-KUF* and its substantially greater conversion percentage of linear fatty acids to 1-alkenes compared to *strain-UndA* and *strain-OP* led us to explore the ability of *strain-KUF* to produce aromatic alkenes, which are high-value commodity chemicals with diverse industrial applications such as in the polymer industry. We found that *strain-KUF* has a notable ability to convert aromatic fatty acids of different chain lengths (**9** to **11**) into the corresponding 1-alkenes (**9a** to **11a**) with 65 to 70% conversion (Fig. 7 and figs. S19 to S21). In contrast, the other two strains exhibited only low activity (1.5 to 8.5% conversion) with these substrates (Fig. 7). To date, there are scant reports on the biosynthesis of aromatic alkenes (*31*). Mostly, these molecules are derived from petroleum resources for commercial use. Our finding of facile biotransformation of fatty acids into commodity aromatic alkenes could lay the foundation of metabolic engineering and the development of chemo-enzymatic cascades toward their bioproduction. Overall, our study demonstrates the remarkable potential of the engineered *strain-KUF* for efficient biotransformation of free fatty acids to medium-chain 1-alkenes (both aliphatic and aromatic) for diverse industrial applications.

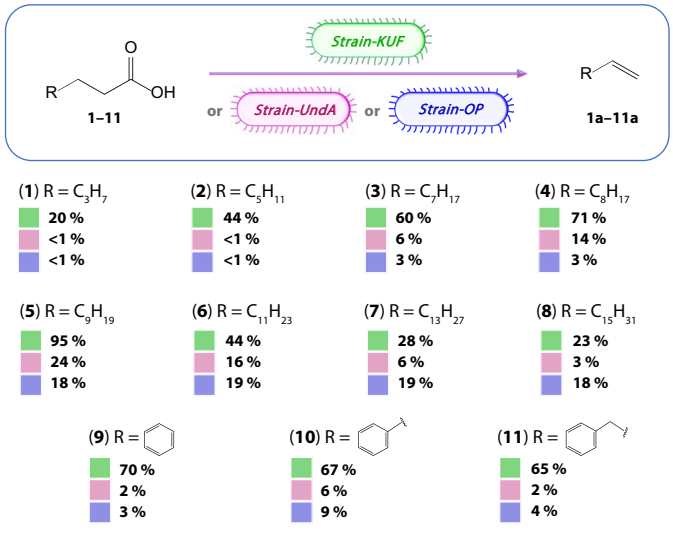

Fig. 7. Biotransformation of aliphatic and aromatic fatty acids to 1-alkenes using whole-cell biocatalysts developed using UndB, UndA, and OleT. Percentage conversion of various aliphatic and aromatic fatty acids to corresponding 1-alkenes by *strain-KUF* (green), *strain-UndA* (pink), and *strain-OP* (blue). Individual percentage conversion values with SDs are reported in figs. S11 to S21.

DISCUSSION

UndB is the only known membrane-bound fatty acid decarboxylase. Despite being more effective than the other fatty acid decarboxylases in producing medium-chain 1-alkenes, the activity of the purified UndB stalled after only 14 TTN within 1 min. Here, we established that the uncoupling of electrons in the UndB reaction resulted in the in situ generation of H_2O_2 that inhibits the UndB reaction. The enzyme activity was revived by introducing catalase to the reaction, demonstrating the reversible nature of the inhibition. Our findings align with the report of Shanklin *et al.* (*30*) on the hydrocarbon-producing aldehyde deformylating oxygenase (ADO), which displayed reversible inhibition by H_2O_2. To counter H_2O_2 inhibition of UndB in vivo, we created a chimeric fusion protein of UndB with catalase, which allowed the degradation of in situ–produced H_2O_2 and sustained UndB activity. It is noteworthy that our chimeric enzyme is a prime example of successfully engineering a membrane enzyme with catalase. In the ADO study, Shanklin *et al.* (*30*) elegantly

proposed the term PIM for minimizing protein inhibition by metabolizing inhibitors. Our strategy of designing and using a chimeric fusion protein to counter UndB inhibition by metabolizing H_2O_2 and converting it to O_2, the cosubstrate of UndB, is a precise illustration of the PIM approach.

Among the 1-alkene–producing fatty acid decarboxylases, H_2O_2 was found to drive the catalysis of OleT, did not affect the activity of UndA, and showed an inhibitory effect on UndB, as described here. These findings underscore the evolution of different mechanistic plots of oxygen activation at the active site of these enzymes. OleT is a close homolog of heme-containing peroxygenases, such as $P450_{BS\beta}$ (CYP152A1), that can use H_2O_2 as the sole source of electrons and oxygen to catalyze the fatty acid decarboxylation reaction (*18*). UndA, conversely, belongs to the emerging superfamily of heme oxygenase-like soluble diiron enzymes, which neither uses H_2O_2 for its catalysis nor gets inhibited by it. This is evident from an early investigation of UndA, where no H_2O_2 was produced in the reaction system, and the addition of catalase did not affect the catalytic activity of UndA (*14*). These findings contrast with our observations demonstrating the inhibitory effect of H_2O_2 on UndB. It was recently reported that H_2O_2 could also support the activity of the membrane-bound stearoyl coenzyme A desaturase (SCD1) (*32*), a prototypical member of the FADS-like superfamily, to which UndB also belongs. SCD1 undergoes the peroxide shunt pathway that does not require biological redox partners to desaturate long-chain fatty acyl CoA (*32*). Unlike SCD1, UndB does not undergo the peroxide shunt pathway; instead, it is inhibited by H_2O_2, highlighting that despite being related to SCD1, UndB operates through a distinct mechanism to ensure the decarboxylation of the fatty acid substrate, very preciously, instead of desaturation or hydroxylation. Our observations could instigate investigation into the other members of FADS-like superfamily, focusing on examining their dependency to, or inhibition by, H_2O_2.

Whole-cell biocatalysts are considered efficient tools for converting bio-based wastes into value-added products. Free fatty acids derived from household and various industrial wastes can be converted into valuable chemicals for a circular economy and sustainability (*33*). Toward this goal, we systematically developed a whole-cell biocatalyst to convert free fatty acids into terminal alkenes with high industrial values. Our approach of protecting UndB from H_2O_2 inhibition in situ by conjugating UndB with catalase and coexpressing the chimeric enzyme with Fdx-FNR in *E. coli* has led to the development of a state-of-the-art whole-cell biocatalyst with an unprecedented efficiency for converting free fatty acids into 1-alkenes.

MATERIALS AND METHODS

Expression and purification of proteins

For the preparation of UndB, the protein was expressed and purified as per our previously published protocol (*17*) with slight modifications as highlighted in the Supplementary Materials. The methods used to express and purify the electron transfer proteins used in this study (Fdxs, FNRs, Pdx, PdR, cytochrome b_5, and cytochrome b_5 reductase) are detailed in the Supplementary Materials. Expression and purification of UndA, OleT, and OleT-AldO were performed following the methods described in the Supplementary Materials.

For the expression of the chimeric KatE-UndB protein, the *KatE* gene of *E. coli* (UniProt ID: P21179) encoding catalase HPII was cloned into a pET-16b(+) vector, followed by the AGCAGCGGT sequence for the SSG linker, followed by the *Pmen_4370* gene (UniProt ID: A4Y0K1) encoding UndB from *Pseudomonas mendocina* (strain ymp), followed by the sequence encoding for 8*His-tag. The initial 24 nucleotides were deleted from the UndB encoding gene to remove the first eight residues. Both the genes used were codon-optimized (GenScript, Singapore) for optimal expression in *E. coli*. The final construct obtained was KatE-SSG-UndB-His_8 (referred to as KatE-UndB for simplification). The full sequence of the chimeric protein can be found in the Supplementary Materials. For the expression of the chimeric protein, *E. coli* BL21(DE3) cells were transformed with the plasmid, and the transformed cells were selected on the lysogeny broth (LB) agar plate containing (100 μg/ml) ampicillin. A single colony from the plate was used to inoculate 10 ml of primary culture in LB medium containing the same antibiotic and grown at 37°C at 220 rpm overnight. A 5-ml primary culture was transferred to 500 ml of terrific broth medium with the same antibiotic. The secondary culture was grown at 37°C at 220 rpm until the optical density at 600 nm reached 0.6, after which the culture was cooled on ice for 10 min, and the protein expression was induced by adding 0.5 mM isopropyl-β-D-thiogalactopyranoside. The culture was then transferred to an incubator shaker at 16°C and grown at 220 rpm for 20 hours. The culture was supplemented with 0.1 mM 5-aminolevulinic acid and 0.2 mM of $(NH_4)_2Fe(SO_4)_2.6H_2O$ during the induction for proper heme and iron incorporation into the protein.

For the purification of KatE-UndB, the culture was centrifuged at 4000*g* for 30 min at 4°C. The harvested cells from 1 liter of culture (~10 to 12 g) were resuspended in 200 ml of lysis buffer [50 mM Hepes (pH 8.0), 200 mM NaCl, 0.5 mM PMSF (phenylmethylsulfonyl fluoride), and deoxyribonuclease I (50 μg/ml)] and lysed by sonication (45% amplitude, 2-s on to 3-s off, 3 cycles of 2 min each) using a sonicator (Q500, Qsonica USA). Cells were kept on ice during the sonication and rested for 5 min between sonication cycles. The cell lysates were centrifuged at 12,000*g* for 10 min at 4°C to pellet the cell debris. The supernatant was collected and centrifuged at 150,000*g* for 65 min at 4°C using the Ti70 rotor in the optima XPN-100 ultracentrifuge (Beckman Coulter, USA) to isolate the membrane fraction.

The isolated membrane fraction was homogenized in 40 ml of hypertonic buffer [50 mM Hepes (pH 8.0), 700 mM NaCl, and 0.5 mM PMSF] and centrifuged at 150,000*g* for 65 min at 4°C to remove the loosely bound peripheral proteins. The resultant brick-reddish colored pellet was homogenized in 20 ml of homogenization buffer [50 mM Hepes (pH 8.0), 200 mM NaCl, 0.5 mM PMSF, and 0.5% (v/v) LMNG (lauryl maltose neopentyl glycol)] and rotated for 1 hour at 4°C. The solution was centrifuged at 25,000*g* at 4°C for 30 min to remove the insoluble particles. The supernatant was incubated with 0.5 ml of cobalt TALON resin (Takara Bio, Japan), pre-equilibrated with the binding buffer [50 mM Hepes (pH 8.0), 200 mM NaCl, and 0.005% (w/v) LMNG] for 2 hours at 4°C. The slurry was transferred to an empty column, and the resin was washed with 20 column volumes (CV) of binding buffer, followed by 20 CV of wash buffer [50 mM Hepes (pH 8), 200 mM NaCl, 0.005% (w/v) LMNG, and 10 mM imidazole]. The protein was eluted from the column using the 3 CV of elution buffer [50 mM Hepes (pH 8), 200 mM NaCl, 0.005% (w/v) LMNG, and 250 mM imidazole]. The eluted fractions were collected and immediately injected into a HiLoad 16/60 Superdex 200 SEC column (catalog no. 28989335, Cytiva, USA) pre-equilibrated with equilibration buffer [50 mM Hepes (pH 8.0), 200 mM NaCl, and 0.002% LMNG]. The

protein was eluted from the column using the same equilibration buffer at the flow rate of 1 ml/min. The eluted fractions from the SEC column were collected, and if required, the protein was concentrated using the Amicon Ultra-15 centrifugal filter unit (catalog no. UFC9050, Millipore, USA). The purity of the protein was analyzed by SDS-PAGE. UV-visible spectroscopic studies of the purified chimeric protein were carried out using a Cary 3500 (Agilent, USA) UV-visible spectrophotometer. The SEC equilibration buffer was used as a blank, and the spectrum of the purified protein was recorded in the 240- to 600-nm range. The concentration of the chimeric protein was determined from the absorbance at 280 nm based on the extinction coefficient (ε_{280nm}) 168,595 M^{-1} cm^{-1} at 280 nm calculated using the ExPasy-ProtParam tool (*34*).

T_m determination of UndB

For the determination of the T_m of the UndB in whole-cell lysates, the *E. coli* cells expressing UndB-SSG-TEV-eGFP-His_8 were grown and lysed as mentioned in the Supplementary Materials. After lysis, the lysates were aliquoted into 0.2-ml polymerase chain reaction tubes and heated at different temperatures using a thermal cycler (C1000 Touch thermal cycler, Bio-Rad, USA). After 5 min of heating, the lysates were diluted fivefold in ice-cold assay buffer [50 mM Hepes (pH 8.0), 200 mM NaCl, and 0.01% (w/v) LMNG]. One hundred fifty microliters of the diluted lysates was used for the activity analysis. The activity assays were performed in a final volume of 0.2 ml, as mentioned below for the purified protein. After completion, the product was analyzed by gas chromatography–mass spectrometry (GC-MS), as mentioned below. The data were normalized with respect to the amount of the product obtained from the lysates heated at 20°C. The T_m values were obtained by fitting the data to the Boltzmann equation using the GraphPad Prism 8 software. The T_m measurements of the purified tag-free UndB were also performed using the same method.

Activity assays of the purified proteins

Standard activity assays of the purified UndB (without H_2O_2 or catalase) were performed in 1.5-ml glass GC-MS vials, and the typical volume of the assays was 0.5 ml. A standard assay mixture contained 5 μM purified UndB, 5 μM Fdx, 3 μM FNR, 0.5 mM lauric acid [prepared in 0.5% (w/v) tergitol NP-10], 100 μM $(NH_4)_2Fe(SO_4)_2{\cdot}6H_2O$, and 2 mM NADPH. The assays were performed in assay buffer [50 mM Hepes (pH 8.0) containing 200 mM NaCl and 0.01% (w/v) LMNG], initiated with the addition of NADPH, and carried out at 25°C for the indicated time points.

To explore the effect of H_2O_2 on the enzyme activity, the above-mentioned assays were carried out in the presence of 1 or 10 mM H_2O_2 (both giving the same results). For the assays performed in the presence of exogenous catalase, catalase (1 mg/ml; catalog no. C9322, Sigma-Aldrich, USA) was introduced in the above-mentioned assays.

For the time course studies and Michaelis-Menten kinetics studies of UndB in the presence of exogenous catalase and the chimeric KatE-UndB, assays were performed in the presence of 0.5 μM UndB or KatE-UndB, 20 μM Fdx, 5 μM FNR, and 2 mM NADPH. For the time course studies, lauric acid was added to the reaction at the final concentration of 500 μM. For the Michaelis-Menten kinetics studies, varying concentrations (2 to 250 μM) of fatty acid substrates were added to the reaction. The assays were performed at 25°C for 10 min to determine the initial rates, quenched, and extracted by adding an equal volume of ethyl acetate. Product analysis was carried out by GC-MS, as mentioned below. Nonlinear data fitting to the Michaelis-Menten equation was performed using the GraphPad Prism 8 software. Methods for the activity analysis of UndA, OleT, and OleT-AldO are described in the Supplementary Materials.

Generation of whole-cell biocatalysts and activity assays

Strain-U and *strain-KU* were generated by overexpressing UndB-SSG-TEV-eGFP-His_8 and KatE-SSG-UndB-His_8 constructs in pET-16b(+), respectively, in *E. coli* BL21(DE3) cells. *Strain-KUP* was generated by coexpressing KatE-SSG-UndB-His_8 in pET-16b(+) plasmid and Pdx and PdR in pACYC-duet plasmid (*26*) in BL21(DE3) cells. *Strain-KUF* was generated by coexpressing KatE-UndB-His_8 in pET-16b(+) plasmid and Fdx and FdR in pCDF-Duet1 plasmid in BL21(DE3) cells. Cloning of FdR gene, synthesized by Genscript (Singapore) after codon optimization, was performed in the pCDF-Duet1 plasmid between Bam H1 and Not 1 restriction sites. Cloning of Fdx gene, synthesized by Genscript (Singapore) after codon optimization, was performed in the pCDF-Duet1 plasmid between Nde 1 and Xho 1 restriction sites. Appropriate antibiotics were maintained during all steps of transformation and expression, using ampicillin (100 μg/ml) for *strain-U* and *strain-KU*, ampicillin (100 μg/ml) and chloramphenicol (40 μg/ml) for *strain-KUP*, and ampicillin (100 μg/ml) and spectinomycin (100 μg/ml) for *strain-KUF*.

For the initial activity analysis of the strains in the static state, the strains were grown, and proteins were expressed as mentioned above for chimeric protein. After 20 hours of growth at 16°C, a 0.5-ml culture was transferred into a gas-tight 2-ml glass vial, and the reaction was started with the addition of 1 mM lauric acid and 1 mM ascorbate (which we found to be sufficient to provide the reducing equivalents to UndB present in the bacterial cells). The reactions were carried out at 25°C for the indicated time points with gentle shaking. The assays were quenched and extracted using an equal volume of ethyl acetate and analyzed by GC-MS, as mentioned below. KatE-UndB protein concentrations in whole cells were quantified using Western blot and the ImageLab software (Bio-Rad, version 6.0.0). Purified KatE-SSG-UndB-His_8 was resolved on a 10% SDS-PAGE gel at varying concentrations. The protein samples from SDS-PAGE were then transferred to a PVDF membrane, and the blots were developed and detected using mouse anti-histidine monoclonal antibodies and rabbit $F(ab')_2$ anti-mouse polyclonal immunoglobulin G antibodies conjugated with horseradish peroxidase as per the manufacturer's protocol (Bio-Rad, USA). ImageLab software was then used to generate a standard curve, correlating the intensity of the protein band with the known concentrations. The concentration of the KatE-SSG-UndB-His_8 in whole-cell samples was measured by comparing the intensity of its band against the standard curve generated above. The same procedure was used to determine the concentration of OleT in *strain-OP* and UndA in *strain-UndA*.

Whole-cell biotransformation of aliphatic and aromatic fatty acids

For the whole-cell biotransformation studies, *strain-KUF* was generated, as mentioned above. *Strain-UndA* was generated by transforming *E. coli* BL21(DE3) cells with pET-28a(+)-TEV plasmid harboring a codon-optimized UndA-encoding gene (cloned at Nde I/Xho I site) from *P. putida* F1 (UniProt ID: A5W7G6). Since UndA exhibited better activity in the presence of ascorbic acid compared to any redox partner proteins (*14*), no redox protein was coexpressed in strain-UndA.

Strain-OP was generated by cotransforming *E. coli* BL21(DE3) cells with a pET-28a(+) plasmid harboring a codon-optimized OleT-encoding gene from *Jeotgalicoccus* sp. ATCC 8456 (UniProt ID: E9NSU2) (*26*) and a pACYC-duet plasmid harboring genes corresponding to Pdx and PdR (*26*). *Strain-OA* was generated by transforming *E. coli* BL21(DE3) cells with pET-15b(+) plasmid harboring a codon-optimized gene encoding OleT-HRV3C site-AldO (cloned at Nde I/Xho I site).

A single transformed colony was used to start a 3-ml seed culture in LB medium. The culture was grown at 37°C at 220 rpm overnight. A 50-µl overnight culture was used to start a 5-ml secondary culture in ZYM-5052 auto-induction medium. The medium was prepared as per the previously published protocol (*35*). The secondary culture was first grown at 37°C at 220 rpm for 3.5 hours, after which 0.5 ml of the culture was transferred to a 1.5-ml gas-tight glass vial and grown at 25°C at 220 rpm for an additional 24 hours. The cultures were supplemented with 1 mM ascorbate and 1 mM aliphatic (**3** to **8**) or aromatic fatty acids (**9** to **11**) prepared in ethanol, except for small chain fatty acids (**1** to **2**) prepared in dimethyl sulfoxide (DMSO). The final concentration of ethanol or DMSO was maintained at 5% (v/v). The product formation was analyzed by GC-MS, as mentioned below.

Product analysis and GC-MS

To analyze the formation of medium- and long-chain aliphatic and aromatic 1-alkenes (**3** to **11**), the reactions were quenched using an equal volume of ethyl acetate, and the products were extracted after centrifugation of the samples at 10,000*g* for 5 min and analyzed by GC-MS. For analysis, 1 µl of the organic layer was injected into the GC-MS system (Agilent, 8890 GC coupled with the 5977B inert plus mass selective detector) equipped with a HP-5MS UI column (Restek, 30 m by 0.25 mm by 0.25 µm; catalog no. 19091S-433UI) using the autosampler (Agilent, ALS-G4513A) in the split mode with a split ratio of 5:1 and a total flow of 6.6 ml/min. The flow rate of the helium carrier gas was maintained at 1.5 ml/min, the inlet temperature was maintained at 160°C, and the interface temperature was maintained at 250°C. The oven temperature was held at 50°C for 4 min, increased to 150°C at 10°C/min, and then increased to 300°C at 25°C/min, at which it was held for 5 min. The mass spectrometer was operated with automatically tuned parameters at the mass range of 50 to 550 mass/charge ratio (m/z). The signals of the 1-alkenes were identified and quantified by comparison with authentic standards (TCI Chemicals, Japan) using the in-built analysis software (OpenLab CDS, Agilent, version 2.6).

The detection and quantification of shorter-chain 1-alkenes (**1** to **2**) were performed using the headspace of the reaction vial. After performing the reactions in 1.5-ml gas-tight vials, the vials were heated at 80°C for 5 min. Then, 1 ml of the headspace was collected using a gas-tight syringe (Agilent, catalog no. 5190-1530) and injected manually into the GC-MS system. The injector temperature was set at 120°C. Helium was used as the carrier gas with a flow rate of 3 ml/min. The temperature of the oven was initially maintained at 30°C for 3 min, followed by the increase in the temperature at 10°C/min to 100°C, and then at 30°C/min to 300°C. The temperature of the oven was held for 3 min at 300°C. The mass spectrometer was operated with automatically tuned parameters, and the acquired mass range was set at $m/z = 50$ to 550. For quantification, the authentic 1-pentene and 1-heptene standards (TCI Chemicals, Japan) were prepared in the ZYM-5052 medium and analyzed by GC-MS, as mentioned above.

The space-fill cartoons of the proteins were prepared using the AlphaFold modeled structures of the proteins. The AlphaFold structures were obtained from the database using the UniProt IDs (mentioned in the Supplementary Materials) of the proteins UndB, Fdx, FNR, Pdxm and PdR. The cartoon structure of the KatE-UndB chimeric protein was modeled by AlphaFold2 using the ColabFold server (*36*, *37*). The figure panels were organized in Adobe Illustrator (versions 26.0 to 27.5).

Statistical analysis

All the statistical analyses were performed and plotted using GraphPad Prism (versions 8). All the data were plotted as mean ± SD. The K_m and k_{cat} values are reported in terms of mean ± standard error of the mean (SEM).

Supplementary Materials

This PDF file includes:

Supplementary Text
Figs. S1 to S28
Tables S1 to S3
References

REFERENCES AND NOTES

1. J. C. Liao, L. Mi, S. Pontrelli, S. Luo, Fuelling the future: Microbial engineering for the production of sustainable biofuels. *Nat. Rev. Microbiol.* **14**, 288–304 (2016).
2. Y. J. Zhou, E. J. Kerkhoven, J. Nielsen, Barriers and opportunities in bio-based production of hydrocarbons. *Nat. Energy* **3**, 925–935 (2018).
3. P. P. Peralta-Yahya, F. Zhang, S. B. del Cardayre, J. D. Keasling, Microbial engineering for the production of advanced biofuels. *Nature* **488**, 320–328 (2012).
4. J. Keasling, H. Garcia Martin, T. S. Lee, A. Mukhopadhyay, S. W. Singer, E. Sundstrom, Microbial production of advanced biofuels. *Nat. Rev. Microbiol.* **19**, 701–715 (2021).
5. R. M. Lennen, B. F. Pfleger, Microbial production of fatty acid-derived fuels and chemicals. *Curr. Opin. Biotechnol.* **24**, 1044–1053 (2013).
6. S. Ray, P. V. C. Rao, N. V. Choudary, Poly-α-olefin-based synthetic lubricants: A short review on various synthetic routes. *Lubr. Sci.* **24**, 23–44 (2012).
7. G. Lappin, *Alpha Olefins Applications Handbook* (CRC Press, 2014).
8. J. Blackwell, J. Bullen, R. Shubkin, Current and future polyalphaolefins. *J. Synth. Lubr.* **7**, 25–45 (1990).
9. H. T. Galvis, K. De Jong, Catalysts for production of lower olefins from synthesis gas: A review. *ACS Catal.* **3**, 2130–2149 (2013).
10. H. Yu, C. Wang, T. Lin, Y. An, Y. Wang, Q. Chang, F. Yu, Y. Wei, F. Sun, Z. Jiang, S. Li, Direct production of olefins from syngas with ultrahigh carbon efficiency. *Nat. Commun.* **13**, 5987 (2022).
11. T. Iqbal, S. Chakraborty, S. Murugan, D. Das, Metalloenzymes for fatty acid-derived hydrocarbon biosynthesis: Nature's cryptic catalysts. *Chem. Asian J.* **17**, e202200105 (2022).
12. K. Liu, S. Li, Biosynthesis of fatty acid-derived hydrocarbons: Perspectives on enzymology and enzyme engineering. *Curr. Opin. Biotechnol.* **62**, 7–14 (2020).
13. M. A. Rude, T. S. Baron, S. Brubaker, M. Alibhai, S. B. Del Cardayre, A. Schirmer, Terminal olefin (1-alkene) biosynthesis by a novel p450 fatty acid decarboxylase from Jeotgalicoccus species. *Appl. Environ. Microbiol.* **77**, 1718–1727 (2011).
14. Z. Rui, X. Li, X. Zhu, J. Liu, B. Domigan, I. Barr, J. H. Cate, W. Zhang, Microbial biosynthesis of medium-chain 1-alkenes by a nonheme iron oxidase. *Proc. Natl. Acad. Sci. U.S.A.* **111**, 18237–18242 (2014).
15. O. M. Manley, R. Fan, Y. Guo, T. M. Makris, Oxidative decarboxylase UndA utilizes a dinuclear iron cofactor. *J. Am. Chem. Soc.* **141**, 8684–8688 (2019).
16. Z. Rui, N. C. Harris, X. J. Zhu, W. Huang, W. J. Zhang, Discovery of a family of desaturase-like enzymes for 1-alkene biosynthesis. *ACS Catal.* **5**, 7091–7094 (2015).
17. T. Iqbal, S. Murugan, K. Rajendran, J. S. Sidhu, D. Das, Unraveling the conversion of fatty acids into terminal alkenes by an integral membrane enzyme, UndB. *ACS Catal.* **13**, 15516–15525 (2023).
18. C. H. Hsieh, X. Huang, J. A. Amaya, C. D. Rutland, C. L. Keys, J. T. Groves, R. N. Austin, T. M. Makris, The enigmatic p450 decarboxylase OleT is capable of, but evolved to frustrate, oxygen rebound chemistry. *Biochemistry* **56**, 3347–3357 (2017).
19. Y. J. Zhou, Y. Hu, Z. Zhu, V. Siewers, J. Nielsen, Engineering 1-alkene biosynthesis and secretion by dynamic regulation in yeast. *ACS Synth. Biol.* **7**, 584–590 (2018).
20. A. I. Benítez-Mateos, A. Schneider, E. Hegarty, B. Hauer, F. Paradisi, Spheroplasts preparation boosts the catalytic potential of a squalene-hopene cyclase. *Nat. Commun.* **13**, 6269 (2022).

21. J. N. Sachs, D. M. Engelman, Introduction to the membrane protein reviews: The interplay of structure, dynamics, and environment in membrane protein function. *Annu. Rev. Biochem.* **75**, 707–712 (2006).
22. C. G. Tate, in *Heterologous Expression of Membrane Proteins* (Springer, 2010), pp. 187–203.
23. A. M. Seddon, P. Curnow, P. J. Booth, Membrane proteins, lipids and detergents: Not just a soap opera. *Biochim. Biophys. Acta Biomembr.* **1666**, 105–117 (2004).
24. F. P. Guengerich, F. K. Yoshimoto, Formation and cleavage of C–C bonds by enzymatic oxidation–reduction reactions. *Chem. Rev.* **118**, 6573–6655 (2018).
25. R. F. Beers Jr., I. W. Sizer, Progressive inhibition of the catalase-hydrogen peroxide system by acetate, chloride and azide. *Arch. Biochem. Biophys.* **60**, 115–125 (1956).
26. A. Dennig, M. Kuhn, S. Tassoti, A. Thiessenhusen, S. Gilch, T. Bülter, T. Haas, M. Hall, K. Faber, Oxidative decarboxylation of short-chain fatty acids to 1-alkenes. *Angew. Chem. Int. Ed. Engl.* **54**, 8819–8822 (2015).
27. S. Matthews, K. L. Tee, N. J. Rattray, K. J. McLean, D. Leys, D. A. Parker, R. T. Blankley, A. W. Munro, Production of alkenes and novel secondary products by P450 $OleT_{JE}$ using novel H_2O_2-generating fusion protein systems. *FEBS Lett.* **591**, 737–750 (2017).
28. B. Zhang, L. J. Rajakovich, D. Van Cura, E. J. Blaesi, A. J. Mitchell, C. R. Tysoe, X. Zhu, B. R. Streit, Z. Rui, W. Zhang, A. K. Boal, Substrate-triggered formation of a peroxo-Fe(2)(III/III) intermediate during fatty acid decarboxylation by UndA. *J. Am. Chem. Soc.* **141**, 14510–14514 (2019).
29. T. H. Yosca, M. C. Langston, C. M. Krest, E. L. Onderko, T. L. Grove, J. Livada, M. T. Green, Spectroscopic investigations of catalase compound II: Characterization of an iron (IV) hydroxide intermediate in a non-thiolate-ligated heme enzyme. *J. Am. Chem. Soc.* **138**, 16016–16023 (2016).
30. C. Andre, S. W. Kim, X. H. Yu, J. Shanklin, Fusing catalase to an alkane-producing enzyme maintains enzymatic activity by converting the inhibitory byproduct H_2O_2 to the cosubstrate O_2. *Proc. Natl. Acad. Sci. U.S.A.* **110**, 3191–3196 (2013).
31. R. McKenna, D. R. Nielsen, Styrene biosynthesis from glucose by engineered *E. coli*. *Metab. Eng.* **13**, 544–554 (2011).
32. J. Shen, G. Wu, B. S. Pierce, A.-L. Tsai, M. Zhou, Free ferrous ions sustain activity of mammalian stearoyl-CoA desaturase-1. *J. Biol. Chem.* **299**, 104897 (2023).
33. P. Intasian, K. Prakinee, A. Phintha, D. Trisrivirat, N. Weeranoppanant, T. Wongnate, P. Chaiyen, Enzymes, in vivo biocatalysis, and metabolic engineering for enabling a circular economy and sustainability. *Chem. Rev.* **121**, 10367–10451 (2021).
34. E. Gasteiger, C. Hoogland, A. Gattiker, S. E. Duvaud, M. R. Wilkins, R. D. Appel, A. Bairoch, *Protein Identification and Analysis Tools on the ExPASy Server* (Springer, 2005).
35. F. W. Studier, Protein production by auto-induction in high-density shaking cultures. *Protein Expr. Purif.* **41**, 207–234 (2005).
36. J. Jumper, R. Evans, A. Pritzel, T. Green, M. Figurnov, O. Ronneberger, K. Tunyasuvunakool, R. Bates, A. Žídek, A. Potapenko, A. Bridgland, Highly accurate protein structure prediction with AlphaFold. *Nature* **596**, 583–589 (2021).
37. M. Mirdita, K. Schütze, Y. Moriwaki, L. Heo, S. Ovchinnikov, M. Steinegger, ColabFold: Making protein folding accessible to all. *Nat. Methods* **19**, 679–682 (2022).
38. J. Hallgren, K. D. Tsirigos, M. D. Pedersen, J. J. Almagro Armenteros, P. Marcatili, H. Nielsen, A. Krogh, O. Winther, DeepTMHMM predicts alpha and beta transmembrane proteins using deep neural networks (2022); https://biorxiv.org/content/10.1101/2022.04.08.487609v1.
39. D. Drew, M. Lerch, E. Kunji, D.-J. Slotboom, J.-W. de Gier, Optimization of membrane protein overexpression and purification using GFP fusions. *Nat. Methods* **3**, 303–313 (2006).
40. T. Iqbal, D. Das, Biochemical investigation of membrane-bound cytochrome b5 and the catalytic domain of cytochrome b5 reductase from Arabidopsis thaliana. *Biochemistry* **61**, 909–921 (2022).
41. W. Zhang, L. Du, F. Li, X. Zhang, Z. Qu, L. Han, Z. Li, J. Sun, F. Qi, Q. Yao, Y. Sun, C. Geng, S. Li, Mechanistic insights into interactions between bacterial class I P450 enzymes and redox partners. *ACS Catal.* **8**, 9992–10003 (2018).
42. B. E. Eser, D. Das, J. Han, P. R. Jones, E. N. G. Marsh, Oxygen-independent alkane formation by non-heme iron-dependent cyanobacterial aldehyde decarbonylase: Investigation of kinetics and requirement for an external electron donor. *Biochemistry* **50**, 10743–10750 (2011).
43. A. Schallmey, G. Den Besten, I. G. Teune, R. F. Kembaren, D. B. Janssen, Characterization of cytochrome P450 monooxygenase CYP154H1 from the thermophilic soil bacterium Thermobifida fusca. *Appl. Microbiol. Biotechnol.* **89**, 1475–1485 (2011).

Acknowledgments: We thank C. Winkler, University of Graz, Austria, for the gift of pACYC*camAB* vector. We thank S. Li, Shandong University, China, for the gift of expression plasmids harboring Fdx and FNR genes. We thank R. P. Hausinger, Michigan State University, USA, for valuable suggestions on the manuscript. **Funding:** This work was supported by the Science and Engineering Research Board (CRG/2023/000760), India, Council of Scientific and Industrial Research (01/3131/23/EMR-II), India, Prime Minister's Research Fellowship (TF/PMRF-22-5658), India, and the Indian Institute of Science (IISc), Bangalore, India (SR/MHRD-18-0021). **Author contributions:** Conceptualization: T.I. and D.D. Methodology: T.I. and D.D. Investigation: T.I. and S.M. Supervision: D.D. Writing—original draft: T.I. and D.D. Writing—review and editing: D.D., T.I., and S.M. **Competing interests:** A patent application has been submitted to the Patent Office, the Government of India, to protect the findings. Patent status: filed; filed by: Indian Institute of Science, Bangalore, India; inventors on the patent: T.I., S.M., and D.D.; date: 09 June 2023; serial no: 202341039729. The authors declare that they have no other competing interests. **Data and materials availability:** All data needed to evaluate the conclusions in the paper are present in the paper and/or the Supplementary Materials.

Submitted 7 October 2023
Accepted 20 May 2024
Published 26 June 2024
10.1126/sciadv.adl2492